Biomolecules and Biomedicine
ISSN: 2831-0896 (Print) | ISSN: 2831-090X (Online)

Journal Impact Factor® (2023): 3.1
CiteScore®(2023):7.4
www.biomolbiomed.com | www.blog.bjbms.org

RESEARCH ARTICLE

Zhu et al: UPP1 and AHSA1 in pancreatic cancer

UPP1 and AHSA1 as emerging biomarkers and targets in pancreatic cancer: A proteomic approach

Kongfan Zhu[1#], Hua Hu[2#], Yuanfa Tao[1], Zhijian Yang[1], Hanjun Li[1*]

[1]Department of Pancreatic surgery, Renmin Hospital of Wuhan University, Wuhan, China;

[2]Department of Bone and Joint Surgery, Renmin Hospital of Wuhan University, Wuhan, China

[#]**Kongfan Zhu** and **Hua Hu** contributed equally to this work.

[*]Correspondence to **Hanjun Li**: lihanjun@whu.edu.cn

DOI: https://doi.org/10.17305/bb.2025.11958

ABSTRACT

The specific protein targets involved in pancreatic cancer (PC) pathogenesis and its varying levels of differentiation remain incompletely understood. Advanced proteomic methodologies provide a powerful means of identifying key regulatory proteins and signaling pathways central to cancer progression. In this study, proteomic analyses were performed on PC tissue samples of different differentiation grades, along with adjacent non-cancerous (para-PC) tissues. Bioinformatics techniques were used to identify differentially expressed proteins (DEPs) and their associated pathways. Key target proteins were validated using the GEPIA database, reverse transcription-quantitative polymerase chain reaction (RT-qPCR), western blotting, immunohistochemistry (IHC), and immunofluorescence (IF). A total of 431 DEPs were identified between PC and para-PC tissues, while 470 DEPs distinguished poorly differentiated from moderately differentiated PCs. Functional enrichment analysis revealed that these DEPs participate in various biological processes and signaling pathways. Five DEPs were common to both comparisons, with UPP1, LACTB, and AHSA1 showing particularly notable differences. UPP1 and AHSA1 were significantly upregulated in PC tissues relative to adjacent tissues and exhibited even higher expression in poorly differentiated PCs compared to moderately differentiated ones. These findings were consistently supported by GEPIA, RT-qPCR, western blotting, IHC, and IF analyses. This study identifies UPP1 and AHSA1 as key proteins linked to PC differentiation and progression, highlighting their potential as diagnostic markers and therapeutic targets. These insights enhance our understanding of the molecular mechanisms underlying PC and open new avenues for precision treatment strategies.

Keywords: Pancreatic cancer; PC; proteomics; differentiated pancreatic cancer; target; experimental validation.

INTRODUCTION

Pancreatic cancer (PC) represents an extremely virulent and fatal neoplasm, anticipated to rank as the runner-up in mortality rates among oncological conditions by the year 2030 [1]. Notwithstanding contemporary progress in detection and therapeutic approaches, the likelihood of pancreatic cancer patients surviving for 60 months does not exceed a tenth, positioning it among the malignancies with the most unfavorable outlook [2]. PC can be classified into well-differentiated (WD), moderately differentiated (MD), and poorly differentiated (PD) types, with poorly differentiated PC exhibiting the highest invasiveness and worst prognosis [3]. The incidence of PC continues to rise globally [4]. Prominent predisposing factors encompass tobacco use, excessive body weight, impaired glucose metabolism, and long-term pancreatic inflammation [5]. At the molecular level, KRAS mutations are a key driver in PC development, present in approximately 90% of patients [6]. Other common genetic alterations involve TP53, CDKN2A, and SMAD4 [7]. While these genetic changes may vary among different grades of PC, our understanding of these variations remains limited. Early diagnosis of PC continues to be challenging. Currently, the gold standard for imaging is dual-phase pancreatic CT scanning, while MRI screening may be beneficial for high-risk populations [8]. However, the development of more sensitive biomarkers for early detection remains a critical unmet need [9].

Proteomics, a rapidly evolving field of research, offers powerful tools for gaining deeper insights into biological systems. Emerging research has underscored the increasing importance of proteomics for identifying cancer targets and developing targeted therapies. Yang et al. utilized an integrated multi-omics approach to pinpoint KDM1A as a potential therapeutic target for patients in the early stages of ESCC [10]. In a separate study, Nam et al. demonstrated that 2-aminoethanethiol dioxygenase (ADO) might function as a potential indicator for prognosis and a viable avenue for treatment in PC [11]. Furthermore, Feng et al. utilized proteomic analysis for uncovering how fucosyltransferase potentially contributes to ESCC development and advancement, thus unveiling a novel target for therapeutic intervention [12].

Mercanoglu et al. employed PNA lectin enrichment and mass spectrometry-based proteomics to investigate the impact of GalNT2-catalyzed O-linked glycan addition on pancreatic growth and physiological roles, offering new insights into the mechanisms of PC pathogenesis [13]. Maebashi et al. utilized proteomic approaches to elucidate the mechanism by which methionine restriction inhibits PC proliferation through suppression of the JAK2/STAT3 pathway, providing novel perspectives for PC

treatment strategies [14]. Bruciamacchie et al. combined single-cell analysis with spatial proteomics techniques to examine how ATR inhibitors enhance the cytotoxic effects of FOLFIRINOX on pancreatic ductal adenocarcinoma by remodeling the tumor microenvironment, presenting new strategies for improving PC therapy [15].

Despite the progress made in PC research, numerous unresolved issues and challenges persist. For instance, the molecular mechanisms underlying PD-PC remain elusive, and further investigation is needed to elucidate its distinctions from PD-PC and MD-PC. Moreover, while proteomics technologies have demonstrated immense potential in cancer research, translating these findings into clinical applications continues to be a significant challenge. To address these issues, we propose the following research hypothesis: Proteomic analysis can reveal molecular differences among poorly and MD-PC, and identify key regulatory proteins and signaling pathways. This study will contribute to elucidating the intricate connections linking PC differentiation to prognosis, as well as provide a foundation for developing novel diagnostic markers and therapeutic targets.

The proposed research methodology involves several key steps. Initially, PC tissue samples of varying differentiation grades will be collected for comprehensive proteomic analysis. Subsequently, advanced bioinformatics techniques, including Weighted Gene Co-expression Network Analysis (WGCNA) and the Mfuzz fuzzy clustering algorithm, will be employed to conduct an in-depth analysis of the proteomic data. This analysis aims to identify crucial protein modules and regulatory networks associated with the degree of differentiation. Finally, the functional significance and clinical relevance of the identified potential target proteins will be confirmed through the integration of information from public databases and experimental validation. This study holds significant scientific and clinical value. Firstly, it will address the knowledge gap in our understanding of PC differentiation mechanisms, providing a comprehensive molecular profile of differentiated PCs. Secondly, by identifying key proteins and pathways correlated with differentiation grades, this research will lay the groundwork for developing novel diagnostic markers and prognostic tools. Moreover, these findings may uncover new therapeutic targets, potentially guiding the development of precision treatment strategies for PD-PC.

MATERIALS AND METHODS

Patients

This study used 22 patients with pancreatic ductal adenocarcinoma collected from Hubei Provincial People's Hospital. Tissue biopsy samples are collected surgically. The biopsy samples are placed in a refrigerated sterile preservation solution and placed on ice packs. Following surgery, samples are accurately labeled, and temperature is controlled during transport. For final preservation, samples are either placed in 10% formalin solution or stored in a -80°C freezer. Among them, 8 PD-PC and 7 MD-PC tissues were used for proteomic testing, and 5 PC tissues were used for Reverse transcription-quantitative polymerase chain reaction (RT-qPCR) and Western blot testing. 1 PD-PC and 1 MD-PC tissues were used for Immunohistochemistry (IHC) experiments. The patient's clinical characteristics are shown in Table 1.

Proteomic analysis

Analysis process

Protein profiling analysis involved detecting the range of peptides in different samples, mapping the identified peptide fragments to their respective protein sequences, and calculating the number of proteins. To evaluate the accuracy of the protein profiling results, we examined the unprocessed mass spectrometry data and calculated the average number of peptides traced and supporting each protein. To ensure data quality, we retained only 7,635 proteins present in >50% of samples in at least one group. For each protein, we applied multivariate normal imputation (MVNI) to impute missing values. Pearson's correlation coefficient analysis and principal component analysis (PCA) were used to compare intra- and inter-group differences. We identified proteomic features by analyzing proteins exhibiting different fold changes (FC) across groups. Differentially expressed proteins (DEPs) were identified based on the criteria: $|\log2(FC)| > 0.263$ and unpaired $p < 0.05$. DEPs were visualized using volcano plots and hierarchical clustering heatmaps. Gene set enrichment analysis (GSEA), Gene Ontology (GO), and Kyoto Encyclopedia of Genes and Genomes (KEGG) pathway enrichment analyses were performed on DEPs to explore their involvement in signaling pathways. We constructed protein-protein interaction (PPI) networks to investigate associations among DEPs. Mfuzz analysis was employed to identify DEP change trends, while WGCNA was used to identify modules enriched with differential proteins.

Sample preparation

The samples were mixed with 8 M Urea/100 mM Tris-Cl and subjected to treatment with water bath sonication. After centrifugation, protein concentration of the supernatant was measured with BCA method.

Protein reduction and alkylation were conducted with TCEP and CAA at 37 °C for 1 h. Urea was diluted below 2 M using 100 mM Tris-HCl (pH 8.0). Trypsin was added at a ratio of 1:50 (enzyme: protein, w/w) for overnight digestion at 37 ℃. The next day, TFA was used to bring the pH down to 6.0 to end the digestion. After centrifugation (12000×g, 15 min), the supernatant was subjected to peptide purification using self-made SDB-RPS desalting column. The peptide eluate was vacuum dried and stored at -20 ℃ for later use.

Mass spectrometry analysis

All samples were analyzed on timsTOF Pro (Bruker Daltonics), a hybrid trapped ion mobility spectrometer (TIMS) quadrupole time-of-flight mass spectrometer. An UltiMate 3000 RSLCnano system (Thermo) was coupled to timsTOF Pro with a CaptiveSpray nano ion source (Bruker Daltonics). Peptide samples were injected into a C18 Trap column (75 μm*2 cm, 3 μm particle size, 100 Å pore size, Thermo), and seperated in a reversed-phase C18 analytical column (75 μm*15 cm, 1.7 μm particle size, 100 Å pore size, IonOpticks). Mobile phase A (0.1% formic acid in water) and mobile phase B (0.1% formic acid in ACN) were used to establish the seperation gradient at a flow rate of 300 nL/min. The MS were operated in diaPASEF mode. The capillary voltage was set to 1500 V. The MS and MS/MS spectra were acquired from 100 to 1700 m/z. The ion mobility was scanned from 0.6 to 1.6 Vs/cm2. The accumulation time and ramp time were set to 50 ms. The diaPASEF acquisition scheme was defined according to the m/z-ion mobility plane using the timsControl software (Bruker Daltonics). The collision energy was ramped linearly as a function of the mobility from 59 eV at 1/K0=1.6 Vs/cm2 to 20 eV at 1/K0=0.6 Vs/cm2.

Peptide and protein identification and quantification

DIA raw data were analyzed with DIA-NN (V1.8.1). Spectra files were searched against the Human protein sequence database (2023-06-19, 20423 entries) downloaded from Uniprot Library-free search was performed according to the DIA-NN manual (https://github.com/vdemichev/DiaNN/). A predicted in silicon spectra library was generated from FASTA database. Specific Trypsin/P was chosen as the digestion method. One missed cleavage was allowed. Carbamidomethylation on cysteine were chosen as fixed modification. Oxidation on methionine and acetylation on protein N-terminal were chosen as variable modifications. The false discovery rate (FDR) value was set to 0.01 for reliable precursor identification. “MBR” and “heuristic protein inference” was enabled. Protein intensities were normalized with MaxLFQ algorithm.

Data analysis

For DIA data quantification, the output file generated by DIA-NN for each sample was processed in the R workspace and used for the downstream analysis. The intensity values were log2-transformed for calculation and statistical analysis. To guarantee the data quality and effectively use the proteomic data, proteins with over 50% missing values in each group were removed. Missing values were imputed with values representing a normal distribution around the detection limit of the mass spectrometer according to multivariate normal imputation (MVNI). To that end, mean and standard deviation of the distribution of the real intensities were determined, then a new distribution with a downshift of 1.8 standard deviations and a width of 0.25 standard deviations was created. The total matrix was imputed using these values, enabling statistical analysis.

In our DIA-MS based proteomics; to identify the differentially expressed proteins between different groups, statistical significance was assessed by unpaired t-test. Proteins with $p < 0.05$ and fold change (FC) > 1.2 or < 1/1.2 were considered to be significantly changed. Functional enrichment analysis of quantified proteins was based on Gene Ontology (GO), Kyoto Encyclopedia of Genes and Genomes (KEGG) pathway database and Hallmark gene sets. Fisher's exact test was used to compare DEPs and background proteins. GO or KEGG terms with a P value < 0.05 and protein counts ≥ 3 were screened out as enriched terms in DEPs. We also conducted GSEA analysis and obtained important gene sets through the following parameters: NES > 1, NOM p value < 0.01, and FDR q value < 0.25. The protein–protein interaction (PPI) network was conducted via STRING database (https://string-db.org/). Interactions with combined score > 0.4 were remained in the network.

GEPIA database analysis

We utilized the Gene Expression Profiling Interactive Analysis (GEPIA) database to analyze the expression levels of Uridine phosphorylase 1 (UPP1), Lactamase beta (LACTB), and Activator of HSP90 ATPase activity 1 (AHSA1) proteins in PC tissues. Data from 179 PC samples and 171 adjacent non-cancerous tissues (para-PC) tissue samples were extracted for comparative analysis. Protein expression levels were quantified using the standard protocols integrated within the GEPIA platform. The analysis of gene expression differences was conducted employing the R package limma, utilizing standard settings. Statistical significance was determined using Student's t-test, with a p-value < 0.05 considered statistically significant. Box plots were generated to visualize the distribution of protein expression levels between PC

and para-PC groups. All analyses were conducted using the integrated tools available on an online gene expression profiling platform for cancer research. The results were further processed and visualized using R software (version 4.0.3, R Foundation for Statistical Computing) with ggplot2 package for enhanced graphical representation.

WGCNA

We obtained RNA-seq data and corresponding clinical information for PC patients from The Cancer Genome Atlas (TCGA) database. Raw count data were normalized using the DESeq2 package (Bioconductor) and log2-transformed. Genes with low expression (counts < 10 in more than 80% of samples) were filtered out. DEPs between tumor and normal samples were identified using the limma package (Bioconductor) with $|\log2FC| > 1$ and adjusted p-value < 0.05 as cutoffs. We then performed WGCNA using the WGCNA R package to construct a gene co-expression network. A soft-thresholding power was chosen based on the criterion of approximate scale-free topology. The topological overlap matrix (TOM) was calculated and hierarchically clustered to identify gene modules.

Mfuzz analysis

For protein expression analysis, we employed the Mfuzz package (version 2.48.0) in R (version 4.0.2) to perform soft clustering. Raw protein expression data was log2-transformed and standardized using the standardize function in Mfuzz. We applied the Mfuzz function to cluster proteins based on their expression patterns across para-PC, PD-PC, and MD-PC groups, using a cluster number (c) of 6 and fuzzifier parameter (m) of 2.5. These parameters were optimized using the mestimate function. Differentially expressed proteins were identified using limma with a false discovery rate < 0.05 and fold change > 1.5. Mfuzz cluster plots were generated using the Mfuzz.plot function.

RT-qPCR

Total RNA was extracted from tissue using TRIzol reagent (Ambion, 15596-026) and reverse-transcribed into cDNA using HiScript II Select qRT SuperMix II (VAZYME, R233) mixed liquor. Thereafter, RT-qPCR was performed using AceQ qPCR SYBR Green Master Mix (VAZYME, Q111) with the corresponding primer sequences (Table 2). Data analysis was performed using the $2^{-\Delta\Delta Ct}$ method.

Western blot

For protein extraction, tissue samples were placed in EP tubes containing RIPA lysis buffer (Servicebio) and homogenized using an automatic grinder (Tissvelyser-24L, Shanghai Jingxin). Following

centrifugation, the supernatant was collected, and protein concentration was determined using the BCA method (Guangzhou JeBest Biotechnology). Forty micrograms of the protein sample were combined with loading buffer and heated at 95°C for 10 minutes. Proteins were then separated by SDS-PAGE using 12% separating and 5% stacking gels. Following electrophoresis, proteins were transferred to PVDF membranes (Millipore). Membranes were blocked with 5% non-fat milk in TBST for 2 hours and then incubated overnight at 4°C with primary antibodies. Primary antibodies included UPP1 (Wuhan Sanying Biotechnology, 1:2000), LACTB (Boster, 1:2000), AHSA1 (Boster, 1:2000), and GAPDH (Affinity, 1:20000). Following washing with TBST, membranes were treated with appropriate HRP-conjugated secondary antibodies (Beyotime Biotechnology) for two hours at ambient temperature. Chemiluminescence detection was performed using ECL substrate (Servicebio), and the membranes were exposed to X-ray film. Protein band densities were analyzed using Image Pro Plus software, with GAPDH serving as an internal control for normalization.

Tissue sections

Tissue samples from 8 PD-PC and 7 MD-PC were processed for histological examination. Samples underwent fixation in a 10% neutral buffered formalin solution, followed by dehydration using an increasing alcohol gradient. Subsequently, the specimens were processed with xylene for clearing and embedded within paraffin blocks. Using a Leica RM 2016 microtome, 4 μm thick sections were obtained and placed onto microscope slides. Sections used in H&E staining, Immunofluorescence (IF), and IHC.

H&E Staining

For H&E staining, sections were deparaffinized in xylene, rehydrated through graded ethanol, and stained with Mayer's hematoxylin (BT-P107, Qisai Biological) for 5 minutes followed by 1% eosin Y (BT-P109, Qisai Biological) for 5 minutes. Stained sections were dehydrated, cleared, and mounted with neutral balsam. Images were captured using a Leica FLEXACAM C1 microscope equipped with LAS X imaging software at 200x magnification. This protocol allowed for clear visualization of nuclear (blue) and cytoplasmic (pink to red) structures, enabling detailed morphological analysis of PD-PC and MD-PC tissues.

IF

For IF, sections were deparaffinized and rehydrated, and heat-induced antigen retrieval was performed using Tris-EDTA buffer (pH 9.0, Qisai Biological) at 95°C for 15 minutes. We performed multiplex immunofluorescence staining using a tyramide signal amplification system. Primary antibodies against

UPP1 (1:100, Sanying), AHSA1 (1:100, Boster), and LACTB (1:100, Boster) were sequentially applied, followed by HRP-conjugated secondary antibodies and tyramide-fluorophores. Between each round of staining, we used microwave treatment to strip the preceding antibodies while preserving the fluorescent signal. Nuclei were counterstained with DAPI (Beyotime). Images were acquired using a multispectral imaging system built upon an Olympus BX53 fluorescence microscope platform. We captured at least three representative fields at 200x magnification for each sample. Image analysis was performed using cellSens Entry software (Olympus) to quantify the fluorescence intensity of each marker. Statistical analysis was conducted to compare protein expression levels between PD-PC and MD-PC samples.

IHC

For IHC, sections using Tris-EDTA buffer (pH 9.0) in a pressure cooker for 15 minutes. Endogenous peroxidase activity was blocked with 3% H2O2. Sections were incubated overnight at 4°C with primary antibodies against UPP1 (1:100, Proteintech), AHSA1 (1:100, Boster), and LACTB (1:100, Boster). After washing, sections were treated with a secondary antibody conjugated to HRP (Dako) for 30 minutes at 37°C. Immunoreactivity was visualized using DAB (Dako), followed by hematoxylin counterstaining. Stained sections were dehydrated, cleared, and mounted. Micrographs were obtained via a BX53 optical instrument from Olympus featuring cellSens Entry software. Protein expression was quantified by measuring the average optical density of positively stained areas using ImageJ software. All staining procedures were performed in triplicate to ensure reproducibility.

Survival analysis

Using the TCGA dataset, patient samples were stratified into low-expression and high-expression groups based on the optimal cutoff values for LACTB, UPP1, and AHSA1 gene expression. These cutoffs were determined using the survey_cutpoint function within the 'surveyor' package in R (version 4.4.1). The optimal cutoff value was calculated based on the Youden index (sensitivity + specificity - 1), which identifies the threshold that maximizes the Youden index statistic, thereby optimizing the differentiation between groups while minimizing the p-value associated with the Kaplan-Meier survival analysis.

Ethical statement

This study was approved by the ethics committee of Hubei Provincial People's Hospital (Approval No. WDRY2024-K188), and followed the Declaration of Helsinki. Informed consent was obtained from all individual participants included in the study.

Statistical analysis

Prism software was utilized for experimental verification statistical analyses. We employed Student's t-test to evaluate differences among pairs of cohorts. A p-value < 0.05 indicated statistical importance.

RESULTS

Proteomics analysis overview

We conducted two proteomic studies. The first compared 5 PC (three poorly differentiated and two moderately differentiated) tissue samples with para-PC tissues. The second compared 8 PD-PC tissue samples with 7 MD-PC tissue samples. These studies identified 64,697 and 65,505 peptides, corresponding to 8,307 and 8,340 human proteins, respectively. The reliability of our results was validated by examining the correlation between peptide and protein counts (Figure 1). In the PC vs. para-PC group, Pearson correlation coefficients exceeded 0.7, and PCA revealed clear separation between PC and para-PC sample groups, with PC samples showing high clustering. A total of 431 DEPs were identified (Supplement table 1), including 332 upregulated and 99 downregulated DEPs in the PC vs. para-PC group (Figure 2A-C). Similar analyses were performed for the PD-PC vs. MD-PC group, where intra-group Pearson correlation coefficients exceeded 0.8. Samples were distributed on opposite sides of the PC1 axis, indicating differences between PD-PC and MD-PC samples. Finally, 470 DEPs were identified (Supplement table 2), with 180 upregulated and 290 downregulated proteins (Figure 2D-F).

Function enrichment analysis of DEPs

Using GO, KEGG, and GSEA, we conducted pathway and functional analyses of the DEPs. In the PC vs. para-PC group, the most significant BP was cell motility, followed by cellular lipid metabolic process and lipid metabolic process (Figure 3A and Figure S1A). The most significant CC was microbody and peroxisome (Figure 3B and Figure S1B). The most significant MF was fatty acyl-CoA hydrolase activity and DNA-binding transcription factor activity (Figure 3C and Figure S1C). Correspondingly, the Peroxisome pathway was the most significant in the KEGG analysis, Alpha-Linolenic acid metabolism and Glycosphingolipid biosynthesis-lacto and neolacto series was the highest path for rich factor (Figure 3D and Figure S1D). In the PD-PC vs. MD-PC group, the most significant BP was immune response, followed by coagulation and regulation of body fluid levels (Figure 3E and Figure S2). The most significant CC was extracellular region and space (Figure 3F and Figure S3). The most significant MF was signaling receptor binding and peptidase activity (Figure 3G and Figure S4). Correspondingly, Complement and coagulation cascades was the most significant KEGG pathway, followed by ECM-receptor interaction, Alcoholic liver disease and Platelet activation (Figure 3H and Figure S5).

Additionally, in the PC vs. para-PC group, the GSEA Hallmark gene sets revealed that the pathways with

the highest NES for upregulated DEPs were Glycolysis (p=3.74e-07) and Angiogenesis (p=7.82e-04), while the pathway with the highest NES for downregulated DEPs was Pancreas beta cells (p=1.36e-03) (Figure 4A). In the PD-PC vs. MD-PC group, the pathway with the highest NES for upregulated DEPs was E2F targets (p=2.74e-07), and for downregulated DEPs, the highest NES pathways were Epithelial mesenchymal transition (p=1.00e-10) and Coagulation (p=1.00e-10) (Figure 4B). Notably, Myogenesis was identified in both the PC vs. para-PC and PD-PC vs. MD-PC groups, although it did not have the highest NES. Based on these results, it is evident that DEPs in both the PC vs. para-PC and PD-PC vs. MD-PC groups are involved in multiple signaling pathways. Through the construction of a PPI network, we found that in the PC vs. para-PC group, the DEPs with the most interactions were SRC (degree = 41), PTEN (degree = 30), and HDAC1 (degree = 25). The BP with the most protein nodes in the PPI network were developmental process (count = 48), lipid metabolic process (count = 43), and multicellular organismal process (count = 42) (Figure 5A-C). Conversely, in the PD-PC vs. MD-PC group, the DEPs with the most interactions were C4B (degree = 88), A2M (degree = 59), and VTN (degree = 58). The BP with the most protein nodes in the PPI network were immune system process (count = 46), immune response (count = 45), and defense response to other organism (count = 39) (Figure 5D-F). From the preceding analyses, it is apparent that the DEPs and their functions differ significantly between the PC vs. para-PC and PD-PC vs. MD-PC groups. However, given the intrinsic connection between differentiated PC and PC, a combined analysis of PC, PD-PC, and MD-PC is warranted to identify critical targets in the progression of PC.

PC coalition analysis

Through PCA, clustering heatmap, and PPI network analysis, we identified both common and distinct key proteins among PC, PD-PC, and MD-PC patients (Figures 6A-C). Ultimately, five DEPs (UPP1, SCYL2, LACTB, AHSA1, and ABHD6) were found to be present in both the PC vs. para-PC and PD-PC vs. MD-PC groups (Figure 6D). Mfuzz analysis of protein expression patterns in para-PC, PD-PC, and MD-PC revealed that proteins in module 3 exhibited a gradually increasing expression trend across these groups (Figure 7A). Therefore, subsequent screening for five DEPs should focus on their association with module 3. Module 3 contained 136 DEPs, which, when intersected with the common DEPs from the PC vs. para-PC and PD-PC vs. MD-PC groups, yielded three DEPs (UPP1, LACTB, and AHSA1) (Figure 7B). WGCNA analysis clustered all differentially expressed proteins into 25 modules (Figure 7C). The three intersecting proteins were enriched in the turquoise module. Correlation analysis of the 25 modules showed

that the turquoise module had a correlation of 0.47 (p=0.038) with other modules, suggesting its crucial role in PC initiation and progression (Figure 7D). To further elucidate the significance of UPP1, LACTB, and AHSA1 as key targets in PC development, we quantified these proteins using proteomic data. As shown in Figure 8, UPP1, LACTB, and AHSA1 levels were higher in PC compared to para-PC, and their expression was elevated in PD-PC relative to MD-PC.

GEPIA database and experimental verification targets

The expression levels of target proteins in PC and para-PC groups were validated using the GEPIA database and Western blot experiments. HE, IF, and IHC experiments were employed to verify the expression levels in PD-PC and MD-PC groups. As shown in Figure 9A, the GEPIA database revealed significantly lower expression levels of UPP1, AHSA1, and LACTB proteins in the para-PC group compared to the PC group. RT-qPCR and Western blot analysis of five pairs of PC tissues and adjacent normal tissues demonstrated significantly higher expression levels of UPP1 and AHSA1 proteins, but lower levels of LACTB protein among PC samples relative to para-PC specimens (Figures 9A, B). To further validate UPP1, LACTB, and AHSA1 as critical targets in PC development, we examined 8 PD-PC and 7 MD-PC tissue samples. HE staining revealed distinct histological features between PD and MD PCs. PD-PC cells exhibited high pleomorphism with notable variations in cell size and shape. Duct-like structures were observed, accompanied by abundant fibrous tissue in the stroma. Both groups showed varying degrees of inflammatory infiltration (Figure 10A). Both IHC and IF experiments consistently demonstrated higher average densities of UPP1 and AHSA1 proteins in PD-PC tissues, while LACTB protein showed higher average density in MD-PC tissues (Figures 10B, C). These findings align with the Western blot results. Although the expression trend of LACTB protein differed from the database, UPP1 and AHSA1 proteins were rigorously and comprehensively proven to be crucial targets in PC development and progression.

Metabolic pathway and survival analyses of UPP1, LACTB, and AHSA1

Based on our previous screening and preliminary verification, we identified UPP1 and AHSA1 as potential marker proteins for PC, exhibiting abnormally high expression in PC patients. While pathway analysis has been conducted, the specific metabolic pathways involving UPP1, LACTB, and AHSA1 remain elusive. Moreover, their impact on PC patient survival outcomes warrants preliminary investigation, despite LACTB demonstrating distinct alterations in PC progression compared to UPP1 and AHSA1. Leveraging KEGG analysis results, we narrowed our focus to the metabolic pathways encompassing UPP1, LACTB,

and AHSA1. Our findings revealed that only UPP1 participates in "PYRIMIDINE_METABOLISM" and "Drug metabolism - other enzymes" pathways, where it is designated as "2.4.2.3" (Figures S6, S7). In the PYRIMIDINE_METABOLISM pathway, UPP1 catalyzes the conversion of uridine to uracil. Similarly, in the "Drug metabolism - other enzymes" pathway, UPP1 facilitates the transformation of 5-Fluoro-uridine to Fluorouracil (5-FU). We performed Kaplan-Meier survival analysis for UPP1, LACTB, and AHSA1 using the TCGA database (Figure 11). The results revealed that patients with high expression levels of UPP1 and LACTB exhibited poorer overall survival compared to those with low expression levels of these genes.

DISCUSSION

In this study, we present a paradigm-shifting proteomic analysis of PC tissues, comparing PC with para-PC, as well as PD-PC with MD-PC. Our findings provide unprecedented insights into the molecular mechanisms underlying PC development and progression, and identify novel biomarkers and therapeutic targets that promise to revolutionize PC management.

Our comprehensive proteomic analysis reveals distinct molecular signatures for PC initiation (PC vs. para-PC) and progression (PD-PC vs. MD-PC), highlighting the complex and dynamic nature of PC development. This aligns with and significantly extends previous studies emphasizing the molecular diversity of PC and how it influences disease advancement and therapeutic efficacy [17, 18]. The identification of DEPs in both comparisons provides an unparalleled view of the proteomic changes occurring during PC evolution, offering a more nuanced and detailed perspective on the disease's molecular underpinnings than previously available [19, 20]. A groundbreaking finding of our study is the identification of UPP1 and AHSA1 as consistently upregulated proteins in PC development and progression, validated across multiple experimental platforms. This observation is particularly significant as it suggests these proteins play crucial roles in both the initiation and advancement of PC. UPP1, involved in pyrimidine salvage pathways, may contribute to the altered nucleotide metabolism characteristic of cancer cells, potentially fueling rapid proliferation. Studies have shown that UPP1 is significantly upregulated in multiple malignant tumors, including lung adenocarcinoma [21], bladder cancer [22], gastric cancer [23], and colorectal cancer [24]. AHSA1, an activator of heat shock protein 90, could enhance the stability of multiple oncogenic proteins, thereby promoting tumor growth and survival [25]. AHSA1 is overexpressed in various malignant tumors, including hepatocellular carcinoma [26], breast cancer [27], and multiple

myeloma [28]. We hypothesize that UPP1 may drive metabolic reprogramming in PC cells, while AHSA1 could act as a master regulator of oncogenic signaling pathways. These mechanistic implications provide a solid foundation for future functional studies and highlight promising therapeutic targets.

Our functional enrichment analysis of DEPs revealed distinct pathway activations between PC vs. para-PC and PD-PC vs. MD-PC comparisons, providing novel insights into the evolving biological processes during PC progression. In the PC vs. para-PC group, we observed significant enrichment in cell motility and lipid metabolic processes, which are critical for cancer cell survival and metastasis [29, 30]. Strikingly, the PD-PC vs. MD-PC comparison showed enrichment in immune response and coagulation pathways, suggesting a profound shift in the tumor microenvironment as the disease progresses to a more aggressive state. These findings align with and extend contemporary research highlighting the significance of the tumor microenvironment in PC advancement and its promise as a treatment avenue [31-33]. Metabolic pathway analysis of UPP1, LACTB, and AHSA1 individually revealed that only UPP1 is involved in metabolism. UPP1 converts uridine to uracil, a process that releases ribose-1-phosphate to supply energy for cells. 5-FU is a common chemotherapeutic agent for treating PC. Therefore, UPP1 not only affects drug metabolism but also supports the metabolic adaptation of cancer cells, suggesting it may be a dual therapeutic target. Our PPI network analysis further corroborated these functional differences, identifying key hub proteins in each comparison. The identification of SRC, PTEN, and HDAC1 as central nodes in the PC vs. para-PC network aligns with their known roles in cancer cell signaling and epigenetic regulation [34, 35]. In contrast, the prominence of immune-related proteins like C4B and A2M in the PD-PC vs. MD-PC network underscores the increasing importance of immune modulation as the disease progresses to a more aggressive state [36, 37]. This shift in network dynamics provides unprecedented insights into the evolving molecular landscape of PC and may guide the development of stage-specific therapeutic strategies. The progressive increase in expression of specific proteins, including UPP1 and AHSA1, from para-PC to MD-PC to PD-PC, as revealed by our Mfuzz analysis, provides compelling evidence for their potential roles as drivers of PC advancement. This finding is particularly significant as it identifies these proteins as potential biomarkers for disease progression and as therapeutic targets across different stages of PC [38, 39]. The consistent upregulation across disease stages suggests that these proteins may be fundamental to the pathogenesis of PC, warranting further investigation into their functional roles.

The validation of our proteomic findings using the GEPIA database and experimental techniques further

strengthens the reliability and translational potential of our results. The consistent upregulation of UPP1 and AHSA1 across different experimental platforms and patient cohorts strongly supports their potential as robust biomarkers and therapeutic targets for PC [40]. Interestingly, we observed a discrepancy in LACTB expression between our experimental results and the GEPIA database findings. Since LACTB expression was not evaluated in databases beyond GEPIA, and only tissue transcription and translation levels were measured without verification of post-transcriptional regulation, this unexpected result underscores the intricate nature of protein expression regulation in neoplastic conditions and highlights the need for further research into the role of LACTB in PC progression. We hypothesize that this discrepancy could be due to post-transcriptional regulation mechanisms or tissue-specific effects. This finding emphasizes the importance of using multiple validation approaches in proteomic studies and opens up new avenues for investigating the regulation of LACTB in PC [41]. Regrettably, the GEPIA database lacks data from non-diseased individuals. Consequently, direct comparisons of UPP1, LACTB, and AHSA1 levels between healthy individuals and PC patients will be performed in future in-depth validation studies.

The identification of stage-specific protein expression patterns and associated pathways provides a novel framework for understanding PC progression and may guide personalized treatment strategies. This aligns with and advances the growing trend towards precision medicine in cancer treatment, where molecular profiling is used to tailor therapies to individual patients [8, 42]. Our findings contribute to this paradigm by offering a detailed proteomic landscape that could inform the development of targeted therapies and personalized treatment regimens. Our study has significant clinical implications, using Kaplan-Meier survival analysis, we identified prognostic significance for UPP1 and LACTB. Our findings indicate that high expression of these genes is associated with poor survival outcomes in patients. The identification of UPP1 and AHSA1 as potential biomarkers could aid in the early detection of PC, addressing one of the major challenges in managing this disease [43]. We envision that these proteins could be developed into blood-based biomarkers for non-invasive PC screening. Furthermore, these proteins could serve as therapeutic targets, potentially leading to the development of novel treatment strategies for PC. For instance, small molecule inhibitors of UPP1 or AHSA1 could be developed as targeted therapies for PC. However, it is crucial to note that the translation of these findings into clinical applications will require extensive validation in larger cohorts and functional studies to elucidate the precise roles of these proteins in PC biology [44].

Despite these promising findings, we acknowledge several limitations of our study. To ensure that research findings better reflect the differences between tumor and non-tumor tissues, rather than inter-individual variability, and to eliminate or minimize the potential impact of environmental factors, thereby more precisely revealing disease-induced biological changes. This study primarily focuses on protein expression differences between tumor tissue and adjacent non-tumor tissue. However, some similar alterations may be present in both tumor and adjacent non-tumor tissues. For instance, the discrepancy observed in LACTB expression trends between our experimental results and the GEPIA database might stem from underlying differences between adjacent non-tumor tissue and genuinely healthy pancreatic tissue, necessitating future validation through comparisons with appropriate healthy controls. The sample size, while sufficient for a proteomic study, is relatively small, and larger cohort studies will be necessary to confirm the clinical utility of our findings, particularly considering the discrepant LACTB expression trends observed between the GEPIA database analysis and the experimental validation phase. Additionally, while we have identified potential biomarkers and therapeutic targets, functional studies will be required to elucidate the precise roles of these proteins in PC biology. Furthermore, our study focused on protein expression levels, and future investigations should consider post-translational modifications and protein-protein interactions to provide a more comprehensive understanding of the PC proteome [45]. We also recognize that our study did not address the potential impact of tumor heterogeneity within individual patients, which could influence proteomic profiles. Future research should focus on functional studies to elucidate the mechanistic roles of UPP1 and AHSA1 in PC. These proteins warrant investigation for their therapeutic applicability using laboratory and animal studies. Furthermore, combining protein analysis findings with data from gene expression and small molecule research is crucial to develop a thorough insight into pancreatic cancer biology.

CONCLUSION

In conclusion, our comprehensive proteomic analysis provides unprecedented insights into the molecular landscape of PC progression, representing a significant advance in the field. The identification of UPP1 and AHSA1 as key players in this process opens up new avenues for biomarker development and therapeutic intervention. Our findings not only extend the current understanding of PC proteomics but also provide a robust foundation for future research.

Conflict of interest: Authors declare no conflicts of interest.

Funding: Authors received no specific funding for this work.

Data availability statement: The data that support the findings of this study are available from https://www.iprox.cn/ (accession number: IPX0011770000).

Submitted: 30 December 2024

Accepted: 27 April 2025

Published online: 09 May 2025

REFERENCES

1. Mizrahi JD, Surana R, Valle JW, Shroff RT. Pancreatic cancer. The Lancet 2020; 395(10242):2008-2020. DOI: 10.1016/S0140-6736(20)30974-0
2. Park W, Chawla A, O'Reilly EM. Pancreatic cancer: a review. JAMA 2021; 326(9):851-862. DOI: 10.1001/jama.2021.13027.
3. Haeberle L, Esposito I. Pathology of pancreatic cancer. Transl Gastroenterol Hepatol 2019; 4:50. DOI: 10.21037/tgh.2019.06.02.
4. Beutel AK, Halbrook CJ. Barriers and opportunities for gemcitabine in pancreatic cancer therapy. Am J Physiol Cell Physiol 2023; 324(2):C540-C552. DOI: 10.1152/ajpcell.00331.2022.
5. Hu J-X, Zhao C-F, Chen W-B, Liu Q-C, Li Q-W, Lin Y-Y, et al. Pancreatic cancer: A review of epidemiology, trend, and risk factors. World J Gastroenterol 2021; 27(27):4298-4321. DOI: 10.3748/wjg.v27.i27.4298.
6. Klomp JA, Klomp JE, Stalnecker CA, Bryant KL, Edwards AC, Drizyte-Miller K, et al. Defining the KRAS-and ERK-dependent transcriptome in KRAS-mutant cancers. Science 2024; 384(6700):eadk0775. DOI: 10.1126/science.adk0775.
7. Hayashi A, Fan J, Chen R, Ho Y-j, Makohon-Moore AP, Lecomte N, et al. A unifying paradigm for transcriptional heterogeneity and squamous features in pancreatic ductal adenocarcinoma. Nat Cancer 2020; 1(1):59-74. DOI: 10.1038/s43018-019-0010-1.
8. Pereira SP, Oldfield L, Ney A, Hart PA, Keane MG, Pandol SJ, et al. Early detection of pancreatic cancer. Lancet Gastroenterol Hepatol 2020; 5(7):698-710. DOI: 10.1016/S2468-1253(19)30416-9.
9. Hristova VA, Chan DW. Cancer biomarker discovery and translation: proteomics and beyond. Expert Rev Proteomics 2019; 16(2):93-103. DOI: 10.1080/14789450.2019.1559062.
10. Yang Q, Wei S, Qiu C, Han C, Du Z, Wu N. KDM1A epigenetically enhances RAD51 expression to suppress the STING-associated anti-tumor immunity in esophageal squamous cell carcinoma. Cell Death Dis 2024; 15(12):883. DOI: 10.1038/s41419-024-07275-4.
11. Nam H, Lee W, Lee YJ, Kim J-M, Jung KH, Hong S-S, et al. Taurine Synthesis by 2-Aminoethanethiol Dioxygenase as a Vulnerable Metabolic Alteration in Pancreatic Cancer. Biomol Ther; 33(1):143-154. DOI: 10.4062/biomolther.2024.086.
12. Feng X, Chen J, Lian J, Dong T, Gao Y, Zhang X, et al. The glycogene alterations and potential effects in esophageal squamous cell carcinoma. Cell Mol Life Sci 2024; 81(1):481. DOI: 10.1007/s00018-024-05534-3.
13. Mercanoglu B, Waschkowski S-A, Neuburg E, Schraps N, Giannou AD, Dreyer B, et al. GalNT2-

mediated O-glycosylation affects pancreas development and function in mice. Sci Rep 2024; 14(1):29760. DOI: 10.1038/s41598-024-80276-7.
14. Maebashi M, Miyake K, Yamamoto J, Sahara K, Akiyama T, Kimura Y, et al. Methionine restriction inhibits pancreatic cancer proliferation while suppressing JAK2/STAT3 pathway. Pancreatology 2024; 25(1):108-117. DOI: 10.1016/j.pan.2024.11.023.
15. Bruciamacchie M, Garambois V, Vie N, Bessede T, Michaud H-A, Chepeaux L-A, et al. ATR inhibition potentiates FOLFIRINOX cytotoxic effect in models of pancreatic ductal adenocarcinoma by remodelling the tumour microenvironment. Br J Cancer 2024; 132(2):222-235. DOI: 10.1038/s41416-024-02904-3.
16. Nakamura K, Kageyama S, Kaldas FM, Hirao H, Ito T, Kadono K, et al. Hepatic CEACAM1 expression indicates donor liver quality and prevents early transplantation injury. The Journal of clinical investigation 2020; 130(5):2689-2704. DOI: 10.1172/jci133142.
17. Collisson EA, Bailey P, Chang DK, Biankin AV. Molecular subtypes of pancreatic cancer. Nat Rev Gastroenterol Hepatol 2019; 16(4):207-220. DOI: 10.1038/s41575-019-0109-y.
18. Rode J. The pathology of pancreatic cancer. Baillieres Clin Gastroenterol 1990; 4(4):793-813. DOI: 10.1016/0950-3528(90)90020-h.
19. Kamisawa T, Wood LD, Itoi T, Takaori K. Pancreatic cancer. The Lancet 2016; 388(10039):73-85. DOI: 10.1016/S0140-6736(16)00141-0.
20. Kwon YW, Jo H-S, Bae S, Seo Y, Song P, Song M, et al. Application of proteomics in cancer: recent trends and approaches for biomarkers discovery. Front Med 2021; 8:747333. DOI: 10.3389/fmed.2021.747333.
21. Li Y, Jiang M, Aye L, Luo L, Zhang Y, Xu F, et al. UPP1 promotes lung adenocarcinoma progression through the induction of an immunosuppressive microenvironment. Nat Commun 2024; 15(1):1200. DOI: 10.1038/s41467-024-45340-w.
22. Du W, Tu S, Zhang W, Zhang Y, Liu W, Xiong K, et al. UPP1 enhances bladder cancer progression and gemcitabine resistance through AKT. Int J Biol Sci 2024; 20(4):1389-1409. DOI: 10.7150/ijbs.83774.
23. Wu Z, Tan J, Zhuang Y, Zhong M, Xiong Y, Ma J, et al. Identification of crucial genes of pyrimidine metabolism as biomarkers for gastric cancer prognosis. Cancer Cell Int 2021; 21(1):668. DOI: 10.1186/s12935-021-02385-x.
24. Wang C, Shi Z, Zhang Y, Li M, Zhu J, Huang Z, et al. CBFβ promotes colorectal cancer progression through transcriptionally activating OPN, FAM129A, and UPP1 in a RUNX2-dependent manner. Cell Death Discov 2021; 28(11):3176-3192. DOI: 10.1038/s41418-021-00810-2.
25. Li W, Liu J. The prognostic and immunotherapeutic significance of AHSA1 in pan-cancer, and its relationship with the proliferation and metastasis of hepatocellular carcinoma. Front Immunol 2022; 13:845585. DOI: 10.3389/fimmu.2022.845585.
26. Zhang J, Ren Z, Zheng D, Song Z, Lin J, Luo Y, et al. AHSA1 promotes proliferation and EMT by regulating ERK/CALD1 axis in hepatocellular carcinoma. Cancers 2022; 14(19):4600. DOI: 10.21203/rs.3.rs-1626018/v1.
27. Shi W, Qi L, You X-B, Chen Y-C, Xu Y-L, Yu W-B, et al. Identification of AHSA1 as a potential therapeutic target for breast cancer: bioinformatics analysis and in vitro studies. Curr Cancer Drug Targets 2022; 22(2):142-152. DOI: 10.2174/1568009622666220114151058.
28. Gu C, Wang Y, Zhang L, Qiao L, Sun S, Shao M, et al. AHSA1 is a promising therapeutic target for

cellular proliferation and proteasome inhibitor resistance in multiple myeloma. J Clin Exp Hematop 2022; 41(1):11. DOI: 10.1186/s13046-023-02672-7.
29. Gabitova-Cornell L, Surumbayeva A, Peri S, Franco-Barraza J, Restifo D, Weitz N, et al. Cholesterol pathway inhibition induces TGF-β signaling to promote basal differentiation in pancreatic cancer. Cancer Cell 2020; 38(4):567-583. e511. DOI: 10.1016/j.ccell.2020.08.015.
30. Cheng C, Geng F, Cheng X, Guo D. Lipid metabolism reprogramming and its potential targets in cancer. Cancer Commun 2018; 38(1):27. DOI: 10.1186/s40880-018-0301-4.
31. Grünwald BT, Devisme A, Andrieux G, Vyas F, Aliar K, McCloskey CW, et al. Spatially confined sub-tumor microenvironments in pancreatic cancer. Cell 2021; 184(22):5577-5592. e5518. DOI: 10.1016/j.cell.2021.09.022.
32. Rodriguez E, Boelaars K, Brown K, Eveline Li R, Kruijssen L, Bruijns SC, et al. Sialic acids in pancreatic cancer cells drive tumour-associated macrophage differentiation via the Siglec receptors Siglec-7 and Siglec-9. Nat Commun 2021; 12(1):1270. DOI: 10.1038/s41467-021-21550-4.
33. Poh AR, Ernst M. Tumor-associated macrophages in pancreatic ductal adenocarcinoma: therapeutic opportunities and clinical challenges. Cancers 2021; 13(12):2860. DOI: 10.3390/cancers13122860.
34. Wu P, Heins ZJ, Muller JT, Katsnelson L, de Bruijn I, Abeshouse AA, et al. Integration and Analysis of CPTAC Proteomics Data in the Context of Cancer Genomics in the cBioPortal. Mol Cell Proteomics 2019; 18(9):1893-1898. DOI: 10.1074/mcp.TIR119.001673.
35. Hessmann E, Johnsen SA, Siveke JT, Ellenrieder V. Epigenetic treatment of pancreatic cancer: is there a therapeutic perspective on the horizon? Gut 2017; 66(1):168-179. DOI: 10.1136/gutjnl-2016-312539.
36. Creighton CJ. Clinical proteomics towards multiomics in cancer. Mass Spectrom Rev 2022; 43(6):1255-1269. DOI: 10.1002/mas.21827.
37. Hussain N, Das D, Pramanik A, Pandey MK, Joshi V, Pramanik KC. Targeting the complement system in pancreatic cancer drug resistance: a novel therapeutic approach. Cancer Drug Resist 2022; 5(2):317-327. DOI: 10.20517/cdr.2021.150.
38. Doll S, Gnad F, Mann M. The case for proteomics and phospho-proteomics in personalized cancer medicine. Proteomics Clin Appl 2019; 13(2):e1800113. DOI: 10.1002/prca.201800113.
39. de Oliveira G, Paccielli Freire P, Santiloni Cury S, de Moraes D, Santos Oliveira J, Dal-Pai-Silva M, et al. An integrated meta-analysis of secretome and proteome identify potential biomarkers of pancreatic ductal adenocarcinoma. Cancers 2020; 12(3):716. DOI: 10.3390/cancers12030716.
40. Boys EL, Liu J, Robinson PJ, Reddel RR. Clinical applications of mass spectrometry - based proteomics in cancer: Where are we? Proteomics 2023; 23(7-8):e2200238. DOI: 10.1002/pmic.202200238.
41. Zeng K, Chen X, Hu X, Liu X, Xu T, Sun H, et al. LACTB, a novel epigenetic silenced tumor suppressor, inhibits colorectal cancer progression by attenuating MDM2-mediated p53 ubiquitination and degradation. Oncogene 2018; 37(41):5534-5551. DOI: 10.1038/s41388-018-0352-7.
42. Daamen LA, Molenaar IQ, Groot VP. Recent Advances and Future Challenges in Pancreatic Cancer Care: Early Detection, Liquid Biopsies, Precision Medicine and Artificial Intelligence. J Clin Med 2023; 12(23):7485. DOI: 10.3390/jcm12237485.

43. Yadav DK, Bai X, Yadav RK, Singh A, Li G, Ma T, et al. Liquid biopsy in pancreatic cancer: the beginning of a new era. Oncotarget 2018; 9(42):26900-26933. DOI: 10.18632/oncotarget.24809.

44. Ramalhete L, Vigia E, Araújo R, Marques HP. Proteomics-driven biomarkers in Pancreatic Cancer. Proteomes 2023; 11(3):24. DOI: 10.3390/proteomes11030024.

45. Pan S, Chen R. Pathological implication of protein post-translational modifications in cancer. Mol Aspects Med 2022; 86:101097. DOI: 10.1016/j.mam.2022.101097.

TABLES AND FIGURES WITH LEGENDS

Table 1. Clinical characteristics

Characteristic	Levels	Overall
Tumor size	386±1443 cm^3	
Location	Head & neck	13
	Body & tail	9
Tumor differentiation degree	Poor	10
	Moderate	12
T stage, n (%)	T1	3
	T2	6
	T3	9
	T4	4
N stage, n (%)	N0	10
	N1	5
	N2	5
	NX	2
M stage, n (%)	M0	15
	M1	7
Bile duct infiltration	YES	5
	NO	17
Duodenal infiltration	YES	5
	NO	17
Perineural invasion	YES	19
	NO	3
Vascular invasion	YES	10
	NO	12
Gender, n (%)	Female	8
	Male	14
Age, n (%)	＜=65	12
	＞65	10
Lymph node metastasis	YES	12
	NO	10
Liver metastasis	YES	3
	NO	19
CEA	5.64±14.4 ng/mL	
CA19-9	1806±2533 U/mL	
Vital status	Live	14
	Dead	8

Table 2. Primer sequences

Name	Primer	Sequence	Size
Homo β-actin	Forward	CCCTGGAGAA GAGCTACGAG	180bp
	Reverse	CGTACAGGTCT TTGCGGATG	
Homo UPP1	Forward	TTCTGGTGGG ATAGGTCTGG	168bp
	Reverse	AGCTCTGCAG AACACAGCAA	
Homo LACTB	Forward	TATGTTCCCGA ATTCCCAGA	249bp
	Reverse	TTTGGCTTCAT TCTCCTGCT	
Homo AHSA1	Forward	CAGCCAGCAC TGAAAACTGA	164bp
	Reverse	ACCAGCTCTT GGGTGGTAAA	

Figure 1

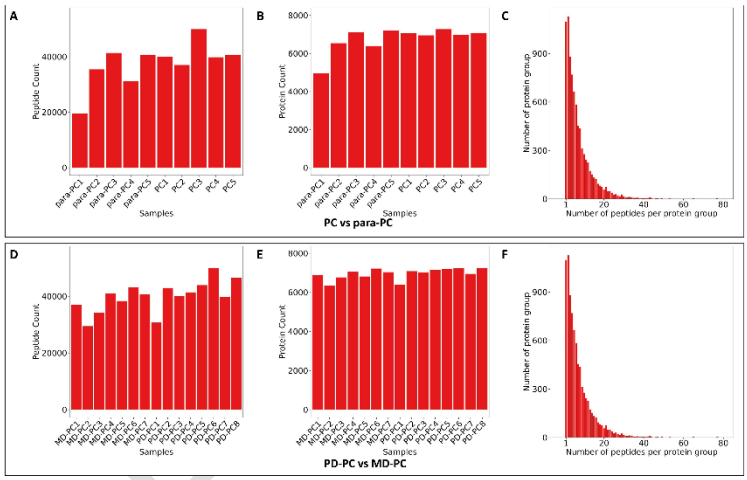

Figure 1. Proteomics analysis overview. (A, D) The distribution of numbers of quantified peptides in detected samples. (B, E) The distribution of numbers of quantified proteins in detected samples. (C, F) The distribution of peptide numbers of quantified proteins.

Figure S2

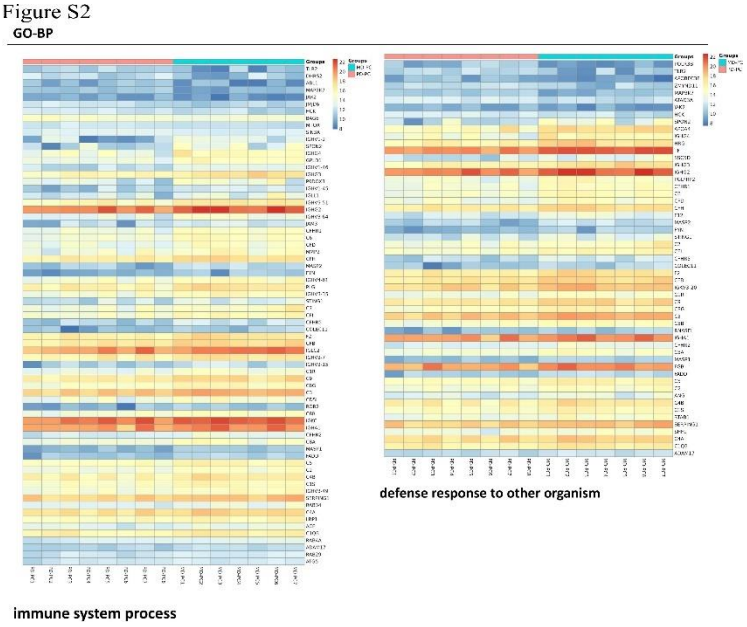

Figure 2. Protein difference analysis. (A, D) Pearson's correlation of protein quantitation. (B, E) Sample repeatability analysis by principal component analysis (PCA). (C, F) Volcano plot showing the differentially expressed proteins (DEPs).

Figure 3

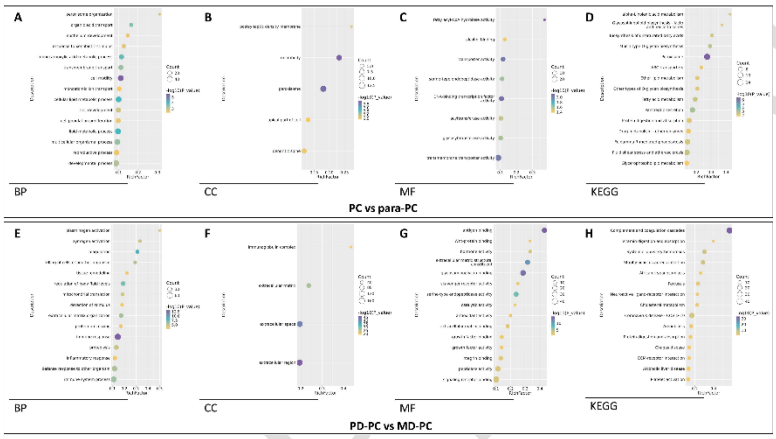

Figure 3. GO and KEGG enrichment analysis of DEPs. (A, E) GO-based enrichment analysis of DEPs shown in the term of biological processes (BP). (B, F) GO-based enrichment analysis of DEPs shown in the term of cellular component (CC). (C, G) GO-based enrichment analysis of DEPs shown in the term of molecular function (MF). (D, H) Kyoto Encyclopedia of Genes and Genomes (KEGG)-based enrichment analysis of DEPs.

Figure 4

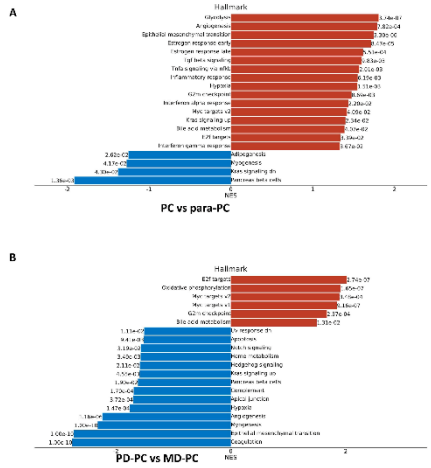

Figure 4. GSEA of DEPs. (A) Hallmark gene set-based enrichment analysis by GSEA between PC group and para-PC group. (B) Hallmark gene set-based enrichment analysis by GSEA between PD-PC group and MD-PC group. NES: Normalized Enrichment Score.

Figure 5

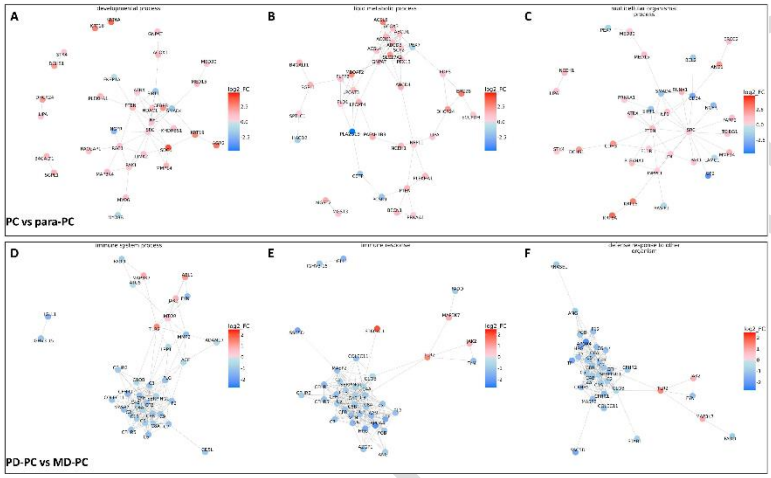

Figure 5. Protein - protein network analysis of DEPs. (A) DEPs in developmental process. (B) DEPs in lipid metabolic process. (C) DEPs in multicellular organismal process. (D) DEPs in immune system process. (E) DEPs in immune response. (F) DEPs in defense response to another organism. Relevance network graph depicting the correlation of proteins derived from DEPs using PPI analysis respectively. Circles indicate the protein ID, Line width indicates interaction strength, red indicates up-regulated proteins, and blue indicates down-regulated proteins. The darker the color, the greater the difference.

Figure 6

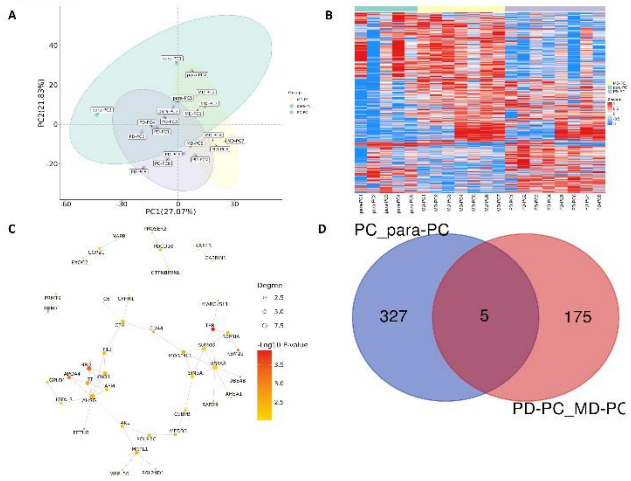

Figure 6. Integrated Analysis. (A) Principal Component Analysis (PCA) of differentially expressed proteins in PC, PD-PC, and MD-PC. (B) Heatmap illustrating quantitative data of differentially expressed proteins in PC, PD-PC, and MD-PC. Each row represents a protein, while each column represents a sample. The color intensity indicates the quantitative data of individual proteins in corresponding samples, displayed as log2-transformed signal intensities. (C) Protein-protein interaction network of differentially expressed proteins in PC, PD-PC, and MD-PC groups, analyzed using the STRING database. Each node represents a differentially expressed protein, with edges between nodes indicating known or predicted protein-protein interactions. Node color denotes the fold change or other relevant scores for each protein, while node size can represent the degree of connectivity within the interaction network. (D) Venn diagram depicting the overlap of DEPs between PC vs. para-PC group and PD-PC vs. MD-PC group.

Figure 7

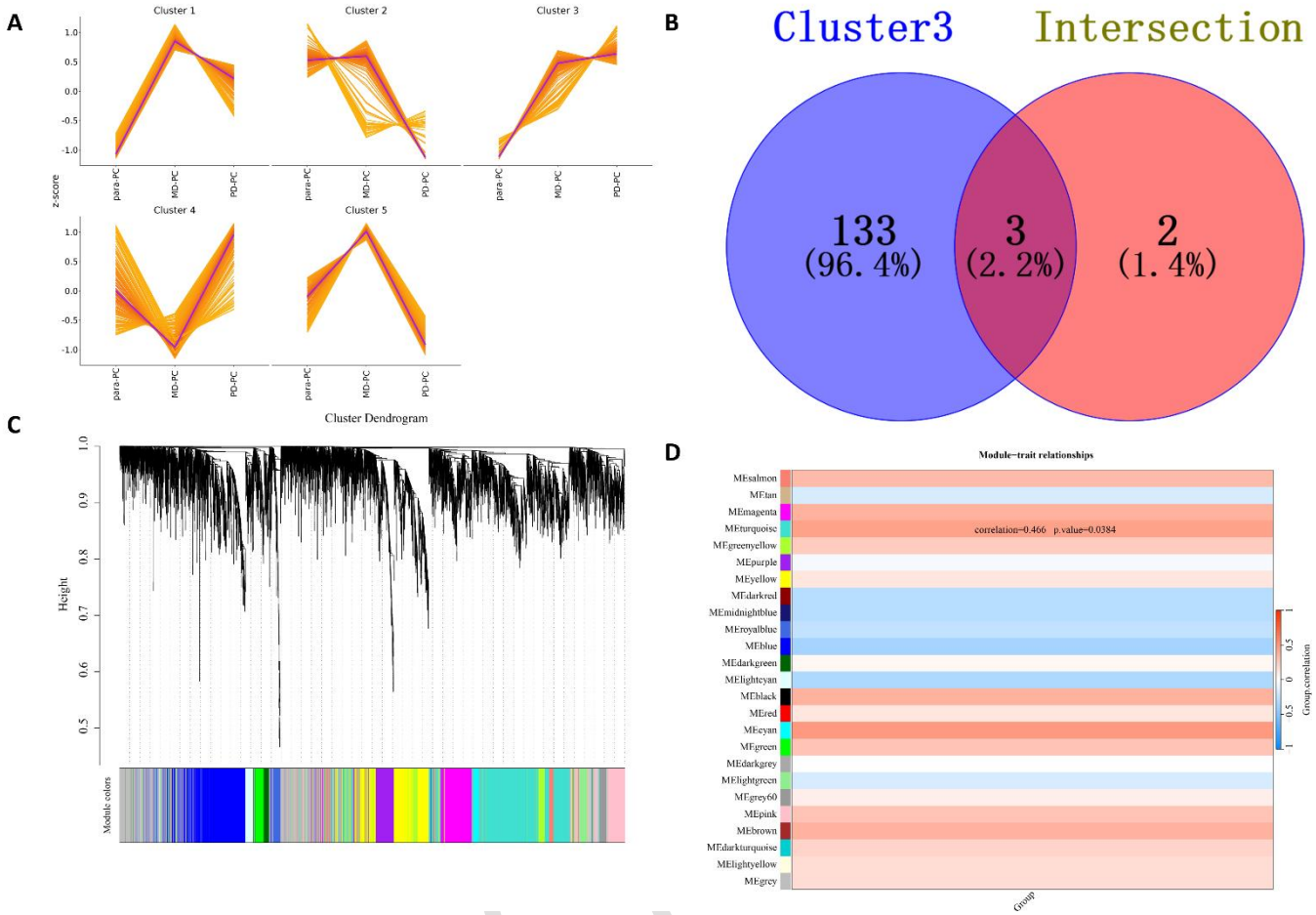

Figure 7. Analysis using Mfuzz and WGCNA. (A) Mfuzz clustering of differentially expressed proteins in para-PC, PD-PC, and MD-PC groups. Each graph represents proteins clustered by similar expression patterns. The x-axis denotes sample groups, while the y-axis indicates relative protein quantification. Each line represents an individual protein, with its shape illustrating the quantitative changes across different sample groups. (B) Venn diagram showing the intersection of 5 proteins with cluster 3. (C) WGCNA analysis. (D) Correlation analysis of 25 modules.

Figure 8

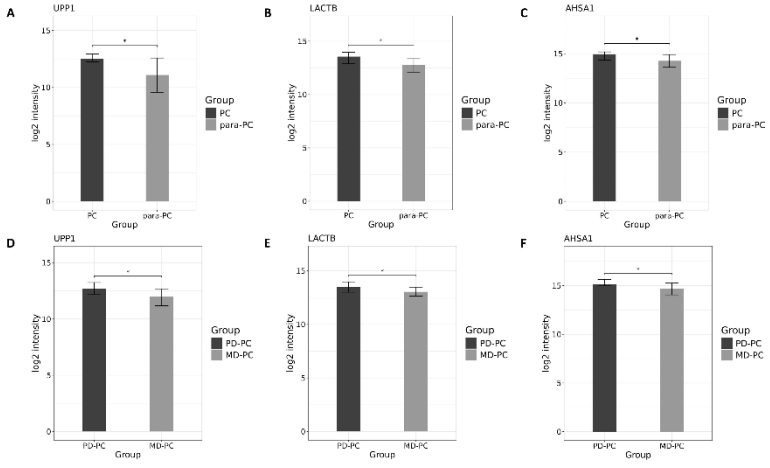

Figure 8. Quantitative expression profiles of UPP1, LACTB, and AHSA1 proteins in omics analysis.

(A-C) Protein quantification values of UPP1, LACTB, and AHSA1 in PC vs para-PC group. (D-F) Protein quantification values of UPP1, LACTB, and AHSA1 in PD-PC vs MD-PC group. *p<0.05.

Figure 9

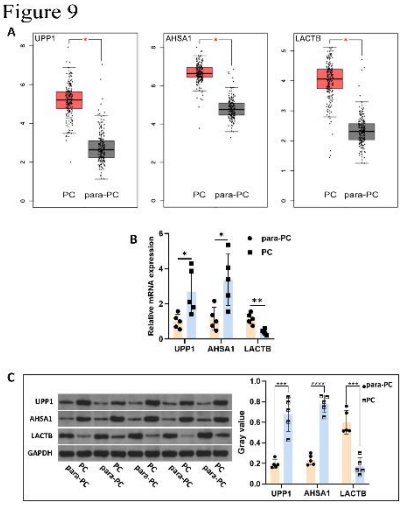

Figure 9. GEPIA database (A), RT-qPCR (B), and Western blot (C) detected the expression of UPP1, AHSA1 and LACTB in PC vs para-PC group. *p<0.05, ***p<0.001, ****p<0.0001.

Figure 10

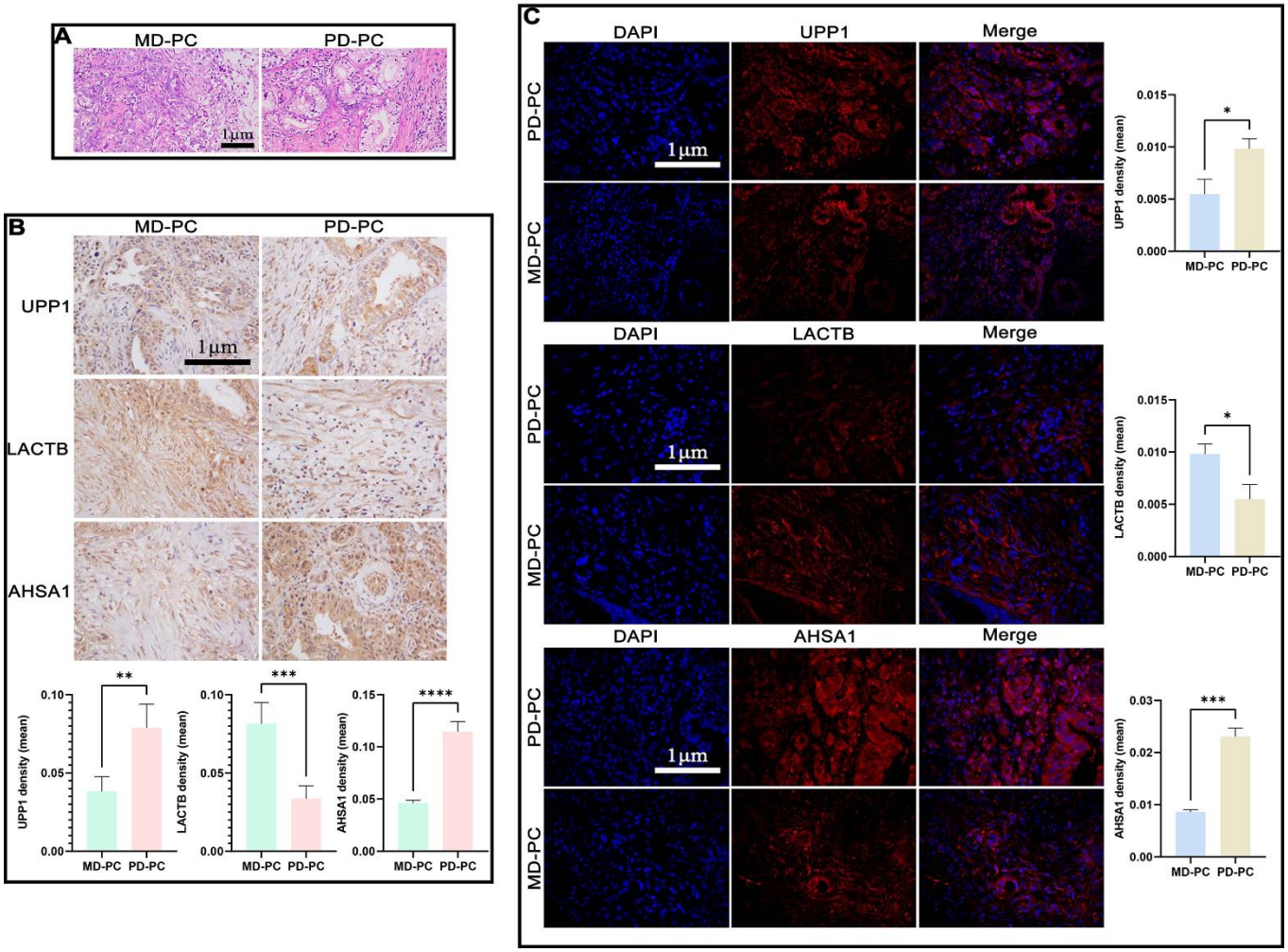

Figure 10. H&E Staining (A), IF (B) and IHC (C) detected the expression of UPP1, AHSA1 and LACTB in PD-PC vs MD-PC group. *p<0.05, **p<0.01, ***p<0.001, ****p<0.0001.

Figure 11

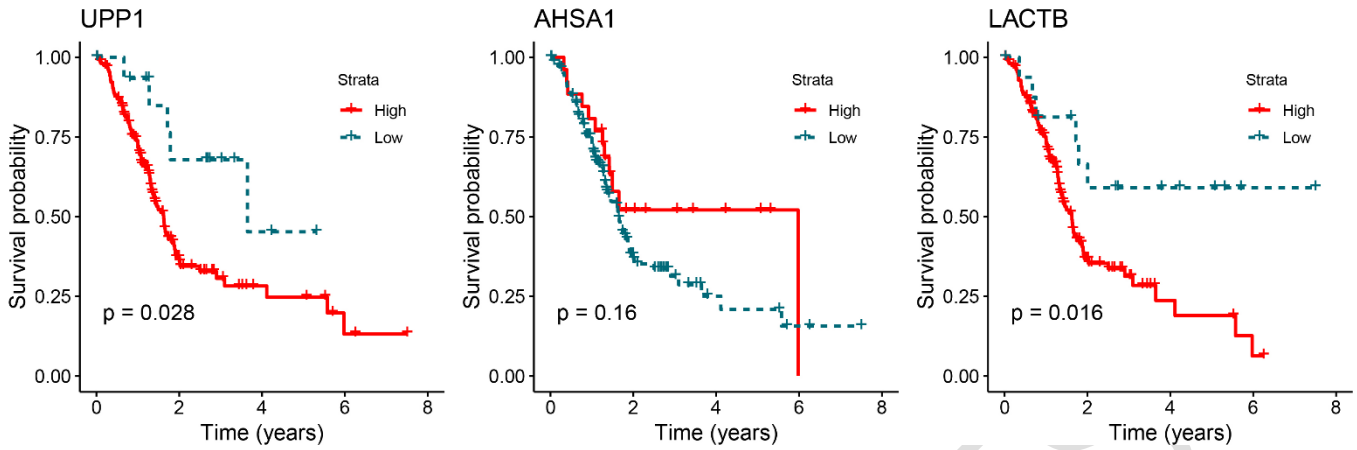

Figure 11. Kaplan-Meier survival analysis.

SUPPLEMENTAL DATA

Supplemental data are available at the following link:

https://www.bjbms.org/ojs/index.php/bjbms/article/view/11958/3872

https://www.bjbms.org/ojs/index.php/bjbms/$$$call$$$/api/file/file-api/download-file?submissionFileId=99998&submissionId=11958&stageId=5

https://www.bjbms.org/ojs/index.php/bjbms/$$$call$$$/api/file/file-api/download-file?submissionFileId=99999&submissionId=11958&stageId=5